sciendo

Reports on Geodesy and Geoinformatics, 2024, Vol. 117, pp. 55–68

DOI: 10.2478/rgg-2024-0007
Received: 5 January 2024 / Accepted: 27 February 2024
Published online: 18 March 2024

ORIGINAL ARTICLE

Accuracy of the application of mobile technologies for measurements made in headings of the Kłodawa Salt Mine

Ewa Joanna Świerczyńska [1*], Damian Kurdek [2†] and Iwona Jankowska [1]

[1]Department of Engineering Geodesy and Measurement Systems, Faculty of Geodesy and Cartography, Warsaw University of Technology, Pl. Politechniki 1, 00-661, Warsaw, Poland
[2]Surveying Department, Salt Mine „Kłodawa" S.A., Aleja 1000-lecia 2, 62-650 Kłodawa, Poland

*ewa.swierczynska@pw.edu.pl
†dkurdek@sol-klodawa.com.pl

Abstract

The "Kłodawa" salt mine, due to geological conditions and continuous salt extraction, is subject to a range of measurements documenting the speed of changes in the geometry of the chambers. Cyclic surveys are conducted under challenging conditions several hundred metres underground. Consequently, measurement methods used for determining the parameters of the ongoing clamping should be of high precision but also be resistant to dense dust (in fields of active mining) and strong gusts (near ventilation shafts).
The research presented here concerns the analysis of the possibilities of solutions offered by modern technologies in mine conditions. Test measurements were conducted at observation stations using linear bases stabilized with metal pins. The base points were located in the aisles, ceiling, and bottom of the chamber in Field 1 of "Kłodawa" salt mine at the depth of 600m. Point clouds mapping the object were acquired using a Leica RTC360 3D laser scanner and two mobile devices: Motorola G100 smartphone and iPad Pro with LiDAR technology using the Pix4Dcatch application. The accuracy of the point cloud from the Leica RTC360 3D laser scanner was determined by comparing it with classic measurements taken with a Leica Disto laser rangefinder. The repeatability and accuracy of the point cloud from a smartphone were examined using statistical analysis based on Pearson's correlation coefficient and cross-correlation. An attempt was also made to approximate the correlation between the obtained errors and two parameters: the number of images and the size of the object.

Key words: convergence, LiDAR, TLS, salt mine, point cloud, iPhone

1 Introduction

In salt mines employing traditional mining methods, symptoms of pit clamping is observed: are bulging pillars or cracked support beams. The first underground observations of these changes began about 100 years ago (Bieniasz and Wojnar, 2007), and the first legal acts regulating the mining of salt deposits in Poland were introduced in the 1960s (Litoński, 1960) and 1970s (Regulation, 1970). The salt mine disaster in Wapno in 1977 contributed to the introduction of detailed regulations (Maj and Florkowska, 2013).

The concept of convergence is defined in literature as a slow and gradual self-clamping of chambers (Kunstman et al., 2002). Its depends on the properties of the rock and the amount of stress in the excavation environment. As model studies have shown, the greatest changes occur in the direction perpendicular to the walls of the chambers. Maximum convergence can be observed at the points of intersection of the axis of perpendicular salt chambers with their walls called *linear principal convergences* (Kortas et al., 2004).

Emerging technologies are commonly used to assess the relative deformations of thechamber, as documented in the study of the

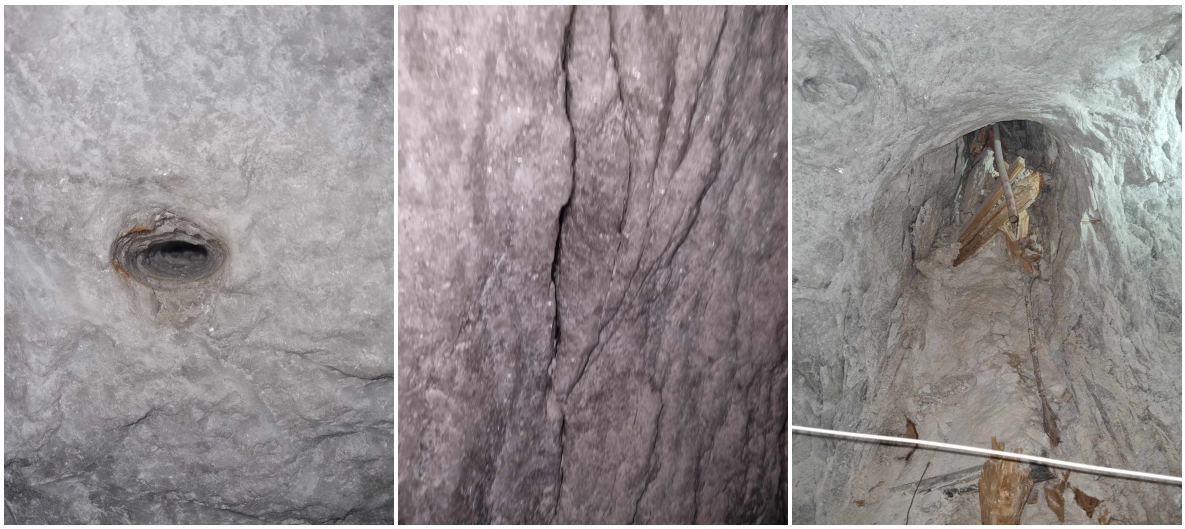

(a) (b) (c)

Figure 1. The effects of the tightening of chambers in a salt mine (visible evidence of the occurrence of convergence): (a) – a hole in the stub; (b) – cracks and fissures on the stubble; (c) – collapsed passage between chambers

frequency and accuracy of changes in the Chapel of St. Kinga, the world's largest underground temple and one of the biggest attractions of "Wieliczka" Salt Mine in Poland, based on 3D photogrammetry, total station and terrestrial laser scanning (TLS) technology (Ochalek, 2018; Lipecki et al., 2016). The authors of the study conclude that measurements of convergence and deformation by laser scanning make it possible to determine the relative deformations of the chapel with sufficient frequency and accuracy. However, the determination of absolute deformations is not possible. They stress that it is reasonable to expand their observations to include measurements within the St. Kinga Chapel and in adjacent chambers. Other researcherswho have measured St. Kinga's Chamber in Bochnia Salt Mine (Szafarczyk and Gawałkiewicz, 2018) notice that laser scanning provides direct information for updating numerical maps, enables the generation of various cross sections, and is a modern tool that allows the measurement of volumetric convergence values. Similar studies were also conducted in Lazy Mine at the mining workplace in the Czech part of the Upper Silesian Coal Basin (Kukutsch et al., 2015).

"Kłodawa" Salt Mine has been mining rock salt in a salt seep since 1956, using the underground method in a pillar-and-chamber system with roof protection. In the "Kłodawa I" mining area, 7 mining fields have been used. At present, mining works are performed in 3 mining fields. These fields are located at the levels from 450m to 810m (Poborska-Młynarska, 2022). In order to observe rock mass movements and their effects, convergence measurements are made in mine workings. The effects of chamber tightening are shown in Figure 1. Visible evidence of the occurrence of convergence are the openings in the floor, which whose section took several years to change from a circular to elliptical, as shown in Figure 1a. The effect of gravity on the chambers is also evidenced by cracks and fissures on the stubble, as shown in Figure 1b, and the collapsed passage between the chambers, as shown in Figure 1c.

One set of the convergence measurements is sidewalk convergence measurements, made at observation stations located in different parts of the fields yearly, involving distance measurements on a stabilised horizontal and vertical base. These observations have been made since 1977, and the measurement accuracy is a several millimetres (approx. 2–3 mm).

Measurements with a hand-held laser rangefinder are performed cyclically to observe changes in the shape of a sidewalk chamber in the horizontal and vertical dimensions (Kurdek, 2020). This method determines two dimensions of the object under study: its width and height. Given that each section of the base is measured three times, and the final section length is the arithmetic average of these three series, the measurement error decreases from ± 2.5 mm (the error of a single measurement) to ± 1.5 mm (the average error of the arithmetic average). In the absence of a determination of the average measurement errors of the Disto rangefinder under real measurement conditions, the results of laboratory determinations are cited, in which the lengths are measured using the rangefinder and interferometer (Maj, 2011). The accuracy of distance measurment with this Disto laser rangefinder is, according to the manufacturer and users, about 2–3 mm in the measurement range up to several tens of metres (Bieniasz et al., 2003).

Convergence of the sidewalk chambers over the annual period averages several millimetres. According to conducted studies, the convergence values of the chambers range from several to a dozen milimetres per year, which means that the reduction in the volume of the pits is significantly slow (Jankowska and Kwaśniak, 2015). For example, the bases on which the experiment was conducted change their lengths by an average of 5–6 mm per year. Compared to the size of the observed phenomenon, the accuracy of manual distance measurement with a laser rangefinder is sufficient.

Crucially, the measurement of distance on a horizontal and vertical bases with a hand-held laser rangefinder makes it possible to determine the changes of chambers' dimensions, their width and height. These are changes in the plane of the vertical section. Therefore, there is a need to develop a method that would allow three-dimensional recording of the state of the chambers. Information is needed about the changes of these objects in all three dimensions of space. The solution to this problem – tachymetric measurement is not always applicable, as the equipment for tachymetric measurement is heavy and thus difficult to transport over long distances, especially when travelling on foot. Thus, there is a need to implement such a method of recording convergence that would be convenient for use in mine conditions, while providing three-dimensional data. Examples of devices that could be used to record cell changes include a smartphone. Similarly convenient are the latest generations of laser scanners, which are much lighter than those manufactured before. naturally, the former would also incur a lower cost than the latter.

Laser scanning is a new technology, but it is already applied increasingly frequently in underground surveys as well. The accuracy of the acquired point clouds depends on the structure of the surface of the measured object from which the laser beam bounces (Su-

chocki et al., 2017), as well as the angle at which the laser beam falls on the measured surface (Świerczyńska and Kołakowska, 2014). If the scanning device has a built-in camera or it is possible to integrate photography with the scanning data then the cloud points have a natural RGB colour in addition to the intensity of the reflection (Woźniak et al., 2015; Świerczyńska, 2020).

Scanning technology is used to measure historical objects and create their 3D models (Suchocki et al., 2023). A relatively new technology for mining surveys involves the use of mobile laser scanning platforms for shaft surveys. They provide the accuracy of 1–3 mm horizontally and 20–100 mm vertically over the entire length of vertical shafts (at 1000 m underground) (Lipecki and Thi Thu Huong, 2020). In addition, the method improves the safety of the measurements and reduces measurement time. The system is suitable for any cage on a mine shaft (Adamek, 2015). Terrestrial laser scanning is also used to determine the negative effects of mining activities on the land surface (Benito-Calvo et al., 2018).

Close range photogrammetry is associated with cameras that are used to take images from a low-altitude aerial vehicle, for example, a UAV, or from the ground. The development of technology has allowed smartphones to be equipped with cameras with significantly improved performance and resolution. It has facilitated using images taken with smartphones in the photogrammetric process of generating point clouds and 3D models. This is an alternative to acquiring 3D data using iPad Pro with LiDAR technology.

In general, thanks to photogrammetric technology, an area of large dimensions (for example, 25 m$\times$55 m) can be recorded with a resolution of 1mm using 2D and 3D reconstruction (Sapirstein, 2016). The accuracy and resolution of the output data depend on the quality of the images taken, the number of those images, the mathematical algorithm for processing the images, and the computational parameters (El-Din Fawzy, 2019). Although laser scanning competes to some extent with photogrammetry, the two technologies are to a large extent complementary, and their integration can lead to more accurate and complete products and open up new areas of application (Baltsavias, 1999).

Low-cost scanning devices, such as the iPhone 13 Pro LiDAR, attracted interest from the scientific community when they became available. They are being tested for use in measuring small-scale objects, such as architectural details (Teppati Losè et al., 2022), cracks (Błaszczak-Bąk et al., 2023), usable areas of small rooms (Zaczek-Peplinska, 2023) and motor vehicles (Kottner et al., 2023). A comparison of the iPad's LiDAR sensor, a handheld laser scanner and traditional forest inventory equipment has already shown a high detection rate for tree trunks over 10 cm in diameter (Gollob et al., 2021).

Other publications describe the effects of measurements during mine shaft inspections using LiDAR technology implanted in a smartphone. Validation using a professional TLS demonstrates the suitability of the iPhone 13 Pro LiDAR scanner for shaft measurement purposes that do not require a high level of accuracy (Rutkowski and Lipecki, 2023).

LiDAR technology involves measuring distances by measuring the timing of the return pulse emitted from the laser transmitter to the laser receiver (Lohani and Ghosh, 2017). Integrating this technology with the smartphone's built-in camera, accelerometer, magnetometer, gyroscope and GNSS antenna has given mobile device users the ability to map surface changes of objects (Jaud et al., 2019; Corradetti et al., 2021).

Terrestrial laser scanners work differently from the iPhone or iPad with LiDAR. In TLS technology, coordinates of points are determined by the distance, the vertical angle, and the horizontal angle. The distance is usually observed by an electro-optical distance measurement (EDM) unit. The EDM determines the distance based on the transit time between emitted and received signals (Dorninger et al., 2008).

In contrast, LiDAR operation on smartphones is based on two principles: structured light (SL) and time-of-flight (ToF). The SL scanning method is based on the principle of triangulation in which incident laser lines are projected onto the object scanned (Huang et al., 2021). A light projector is placed at some distance from the centre of the pinhole camera's projection. The projector emits a plane of light that intersects the scene surfaces in a flat curve called stripes, which is observed by the camera. Two types of ToF technologies are used in LiDAR for smartphones: indirect ToF (iToF) and direct ToF (dToF). The iToF is a depth sensor that measures the distance from the scene to the camera pixels. This measurement is made by illuminating the entire scene with a flash of light, determining the phase between emitted and reflected light. The dToF is an image sensor that has a Lumentum laser with a vertical-cavity emitting-surface (Błaszczak-Bąk et al., 2023).

Due to the difference in measurement technology, TLS has a longer distance measurement range than that of a smartphone with LiDAR. For example, the Leica TCR 360 has a distance measuring range of up to 130 meters, according to the specifications. By comparison, according to the specifications, the maximum measurement range of the iPhone 12 Pro is up to 5 meters.

The aim of this work was to determine the accuracy of recording bases stabilized in salt mine sidewalk chambers using a terrestrial laser scanner and a smartphone. An additional objective was to assess the feasibility of determining convergence using object mapping technologies with point clouds.

The paper is organized as follows: In section 2, we present a description of the conditions in the sidewalk chamber, the specifications of the equipment used in the study, and the characteristics of the acquired data. In section 3, the methodology of the research and the theoretical aspects of the statistical analyses are laid out. Section 4 describes the results of the research in the following subsections: a comparison of methods, a search for correlations between the obtained errors and the two defined parameters, and an analysis of cross-sections of point clouds obtained from a laser scanner and a smartphone. In section 5, we include a discussion of the results of the comparison of the methods used and their reflection in existing studies using similar technologies. In section 6, a summary and concluding remarks are presented.

2 Equipment and data acquired

The test measurement of convergence under mine conditions involved recording the shape of three bases of one of the chambers located in "Kłodawa" salt mine. The test chamber, as shown in Figure 2, has an average width of about 4 m and a height of about 4 m. Four points were installed in the sidewalk chamber for each of the three bases: the left and middle bases, which can be seen in Figure 2a, and the right base, as in Figure 2b.

The test object is located in Field 1 at 600 m level, which has not been used for mining since the 1980s. This means the location features a natural process of squeezing pitsand is free from any influence of mining works from neighbouring fields. There are also constant microclimate conditions in the study area, with an average temperature of 26°C and air flow at 0.3m/s. The observation stations are located in the main haulage roadway, between the cuboid chamber KS-7 and KS-8, which have an average width of about 15 m, a height of about 15 m and a length of about 90 m.

During the test measurements in salt mine "Kłodawa", the chamber was recorded using four measurement technologies:

- method 1: measuring two sections of each of the three bases with a Leica Disto laser rangefinder (with a single distance accuracy of $\pm$2.5 mm) in three series,
- method 2: laser scanning with a Leica RTC360 scanner (with a point position accuracy of $\pm$1.9 mm) from four sites (each site in one series),
- registration of each of the three bases with a Motorola G100 smartphone using the Pix4Dcatch application in three series,
- method 4: registration of each of the three bases with an iPad

(a) (b)

Figure 2. The sidewalk chamber where the test measurements were conducted: (a) – left and middle base view; (b) – right base view

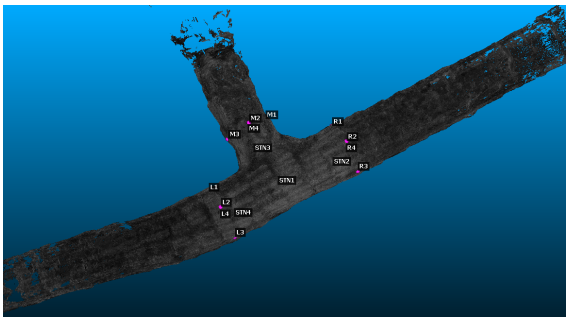

Figure 3. Point cloud (top view) from Leica TRC360 laser scanner, which maps the chamber with the points of the three bases marked: points for L1 to L4 – left base, for R1 to R4 – right base, for M1 to M4 – middle base

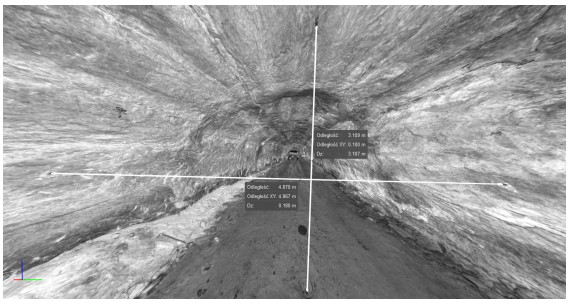

Figure 4. Point cloud in Leica Cyclone REGISTER 360 PLUS software (view from inside the cloud) from Leica TRC360 laser scanner, which maps the chamber with marked sections of the left base

Pro (11 inches, 3rd generation), using the Pix4Dcatch and 3d Scanner app in several series.

For measurements by method 3 and 4 car lamp light was used, and for measurements by method 1 and 2 – only headlamps.

During the test measurements, the chamber was scanned with a Leica TRC360 laser scanner from four stations. The measurements resulted in a point cloud, the visualization of which is shown in the Figure 3. Points STN1, STN2, and STN3 marked the location of the scanner stations. Station 1 was located at the junction of the sidewalk chambers, while the next three were located at each of the three bases. Points L1 to L2 marked the location of the left base points, R1 to R2 marked the location of the right base points, and M1 to M2 marked the location of the middle base points.

The average density of the point cloud, which was created after calibrating all four scans, is significantly high. In the vicinity of the bases, it is about 1 million points per m^2, which means that the distance between adjacent points of the cloud is equal to about 1 mm. Each of the bases was stabilised with metal rods with a diameter of 1cm, which protrude from the walls of the chamber by, on average, 5–6 cm. With such a high density of the resulting point cloud, the survey marks are clearly visible on the scan, allowing for an easy identification of their centres and high accuracy in measuring the lengths of the base sections. As shown in Figure 4, the point cloud from the Leica TRC360 laser scanner was analysed in Leica Cyclone REGISTER 360 PLUS software, which allows the measurement of base sections and the determination of base point coordinates in the local coordinate system.

Mapping chambers in mines with point clouds using laser scanners is a solution already in use. The purpose of this research was to test a relatively new device, the Leica TRC360 scanner, under mine conditions. Subsequent measurements were realized with a more innovative solution, using a smartphone and an iPad (method 3 and method 4). The work in the mine consisted of recording of the aisles, ceiling and bottom of the chamber with low-cost mobile devices, as shown in the Figure 5. Figure 5a shows registration with a Motorola G100 smartphone and Figure 5b shows registration with a iPad Pro with LiDAR.

The point clouds acquired by Method 3 were generated by photogrammetric processing of images taken with a Motorola G100 smartphone equipped with Pix4Dcatch software. Post-processing was performed in Pix4Dcloud or Pix4Dmatic software. Image registration was performed by moving the smartphone along the object. During registration, the smartphone was rotated so that the surface of its screen was approximately parallel to the surface of the object. In this way, the number of oblique images was reduced. The trajectory line of the device's movement staggered a circle. An example of the resulting point cloud, which was created using a smartphone, is shown in Figure 6. The blue triangles denote the positions of the camera at the moments when the images were taken. It can be seen that they represent points approximately lying on an ellipse. Green conesindicate the positions of the base points (metal bars).

Based on the data from a single measurement series, a point cloud was determined that maps a section of the chamber (a slice about 1m in width) containing all four base points. The average density of each point cloud is a quarter of the density of the point cloud acquired with the laser scanner. It averages 250,000 points per m^2, which means that the distance between neighbouring points of the cloud is about 2 mm. Such point cloud density is sufficient to unambiguously identify the metal rods in the chamber walls and their centre points. Figure 7 confirms this with a visualization of one of the points of the left base on the stubble. On the left side of Figure 7 there is a point cloud acquired by photogrammetric method (from Motorola G100 photos) with Pix4Dmatic. On the right side of Figure 7 there is a photo taken with a Motorola G100 smartphone.

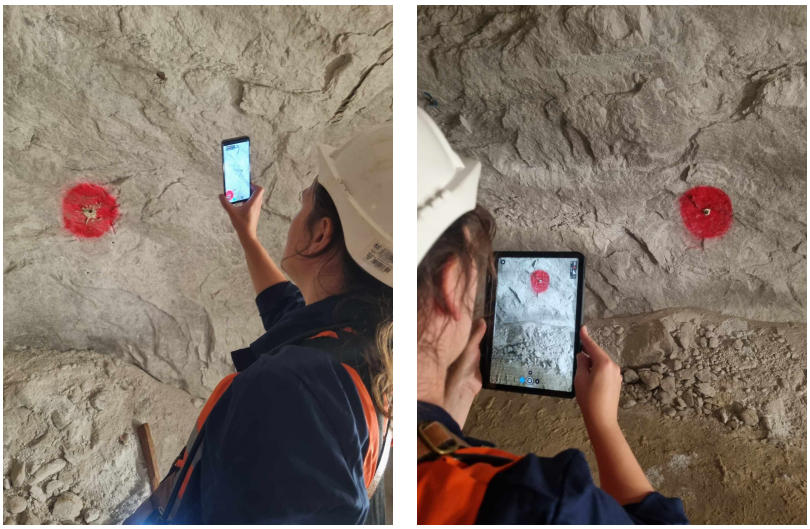

(a) (b)

Figure 5. Proposed work in the mine – recording of the aisles, ceiling and bottom of the chamber with low-cost mobile devices: (a) – Motorola G100 smartphone; (b) – iPad Pro with LiDAR

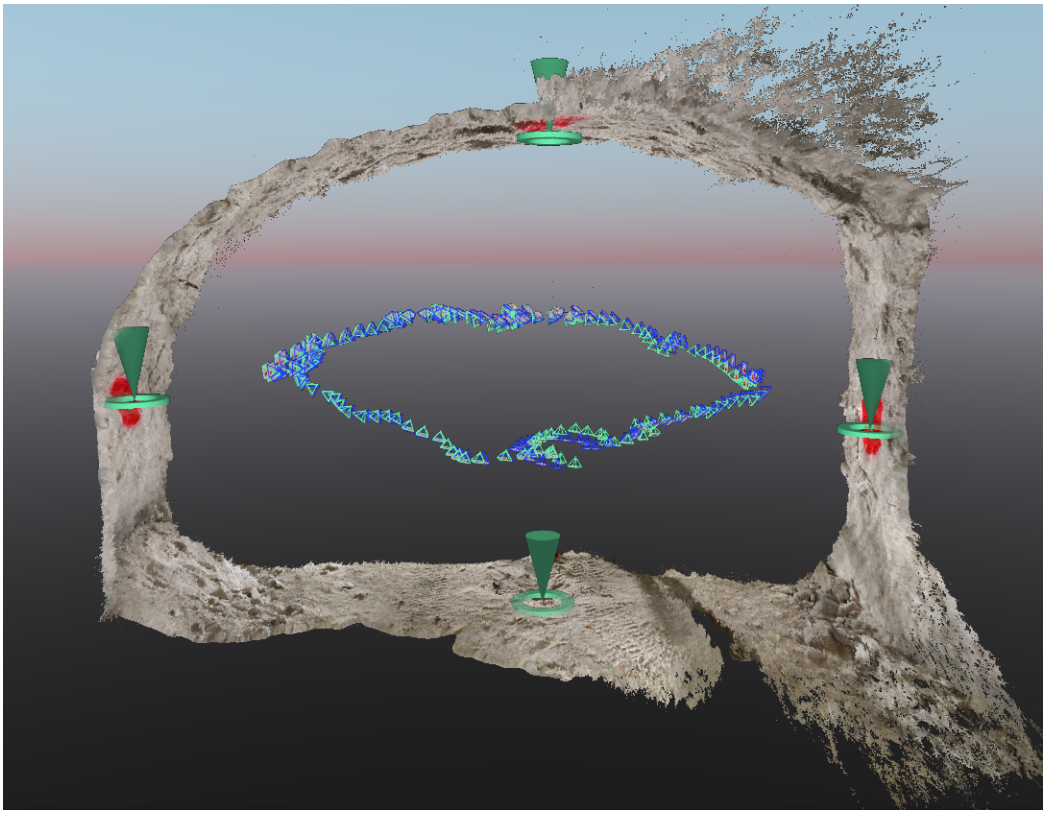

Figure 6. Left chamber: point cloud, acquired by photogrammetric method (from Motorola G100 photos) using Pix4Dmatic software, with marked base points (green colour) and camera positions (blue colour)

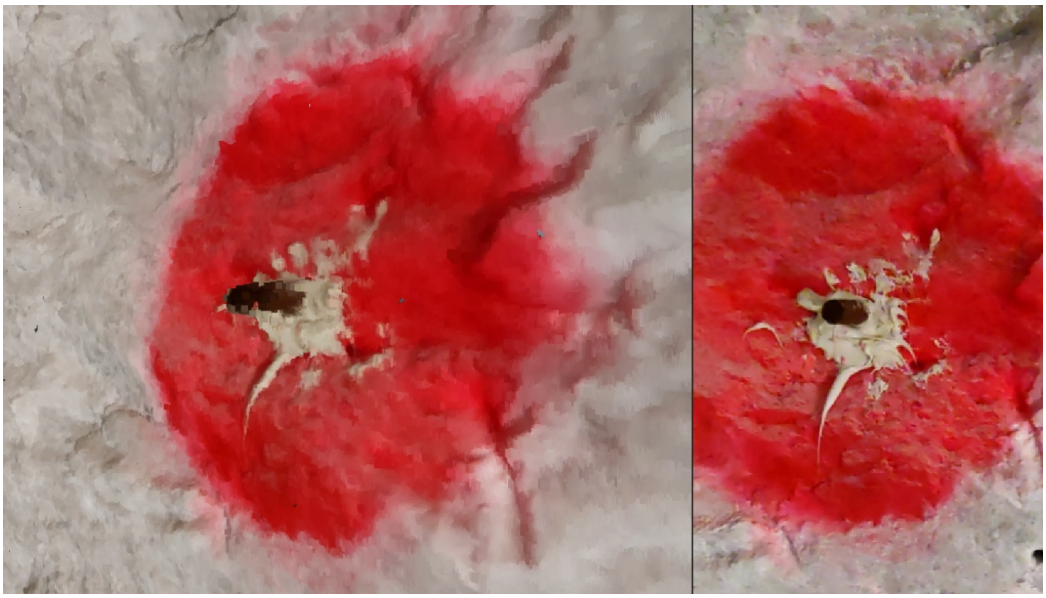

Figure 7. One of the points of the left base on the stubble: left - point cloud acquired by photogrammetric method (from Motorola G100 photos) with Pix4Dmatic, right - photo acquired with Motorola G100 smartphone

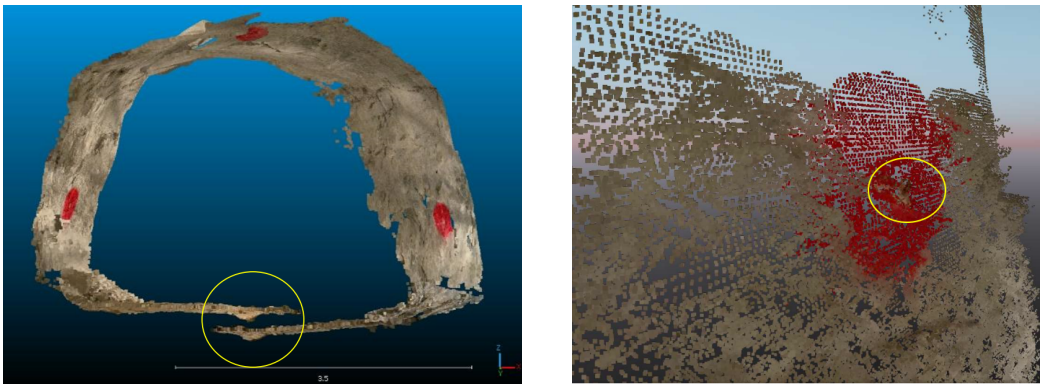

(a) **(b)**

Figure 8. Point cloud from iPad Pro with LiDAR technology using the Pix4Dcatch: (a) – a whole base with visible displacement of the cloud on the right relative to the cloud on the left, (b) – a fragment of the cloud mapping one of the four points of the base

During test measurements, several attempts were made to record each base using the iPad Pro with LiDAR technology. The performance of several applications was assessed. The greatest completeness of the data was obtained by registering the object with the Pix4Dcatch and 3d Scanner applications. Unfortunately, the results obtained did not meet the accuracy requirements of the issue. Mine conditions proved too severe to determine a continuous point cloud of the entire base. In each measurement there was a break in the continuity of the data, which can be observed in the point cloud image as a shift of the beginning of the cloud relative to the end of the cloud, marked with a yellow circle in Figure 8a. In addition, the quality of the obtained point clouds, their density and homogeneity, made it impossible to identify the metal bars on them. The indistinct representation of the metal bar is marked with a yellow circle in Figure 8b.

In the article, the method is described in Equipment and data acquired section to emphasize the fact that it has been attempted. The obtained data were insufficient for analysis, which, as the authors speculate, may be due to the homogeneity of the measured object, the lack of light in the mine and the specific oval shape of the object.

3 Research methodology

The analysis of the acquired data followed the procedure presented in Figure 9. First, the accuracy of point clouds from Leica TRC360 laser scanner (method 2) was evaluated by comparing it with data from Leica Disto laser rangefinder (method 1). This step confirmed the validity of considering laser scanning (method 2) as a reference method in relation to data from Motorola G100 smartphone using the Pix4Dcatch application (method 3). In the next part of the study, the length errors of the base sections were calculated from Motorola G100 smartphone data and Leica TRC360 laser scanner data. The point clouds were also compared globally.

The accuracy of the data and the correlation between the defined parameters were determined using formulas commonly used in statistics.

The accuracy of a measurement with an instrument is often determined by relative error, which is the division of the difference between the measured and real values to the measured value:

$$\delta(x) = \frac{|x - x_0|}{x} \cdot 100\% \tag{1}$$

where x is the measured value, x_0 is the real value.

This parameter is used to determine the scale of the object model

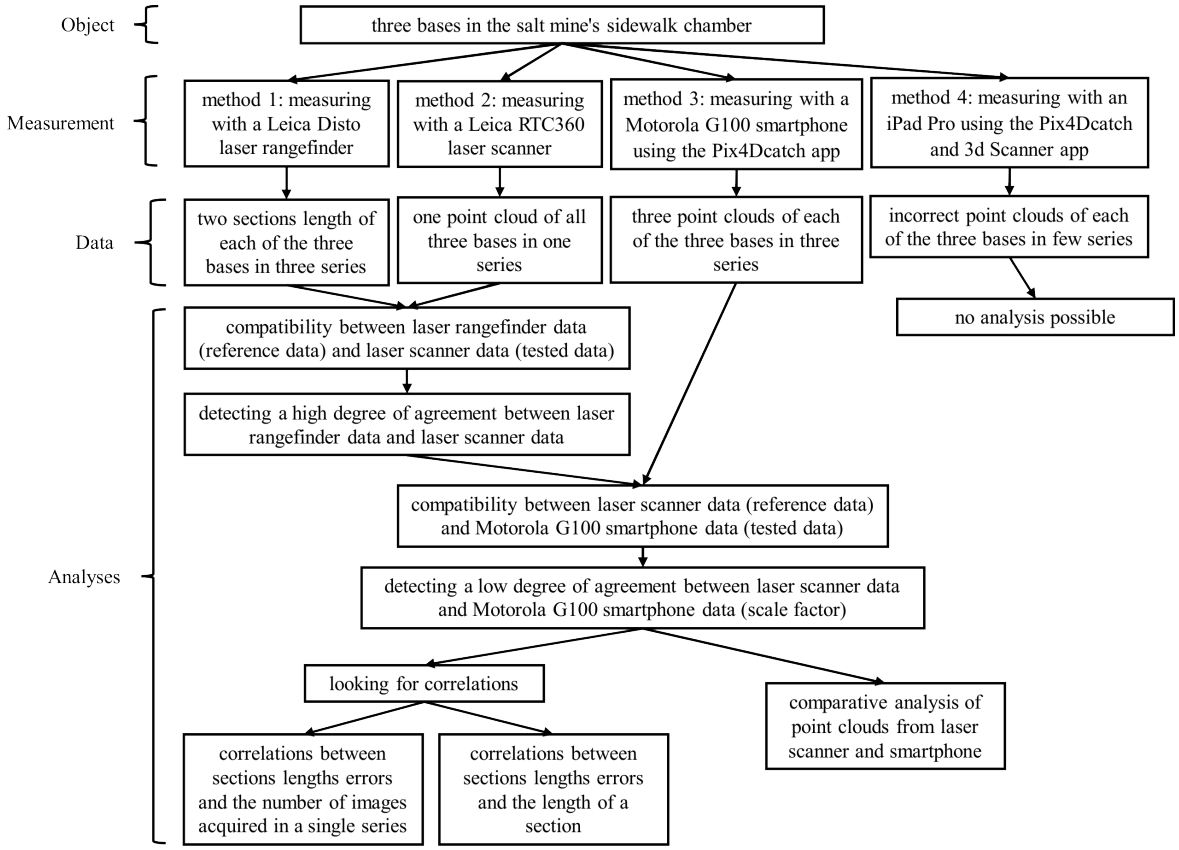

Figure 9. Measurement and analysis procedure

that was created from the measurement data (Miller et al., 2022).

A measure of linear dependence of two random variables is their correlation coefficient (Teukolsky et al., 1992). If each variable has N scalar observations, then Pearson's correlation coefficient is defined as:

$$\rho(A,B) = \frac{1}{N-1}\sum_{i=1}^{N}\left(\frac{A_i-\mu_A}{\sigma_A}\right)\left(\frac{B_i-\mu_B}{\sigma_B}\right) \tag{2}$$

where μ_A and σ_A are the mean and standard deviations of A, respectively, and μ_B and σ_B are the mean and standard deviations of B (Pearson, 1896).

The correlation coefficient matrix of two random variables is the matrix of correlation coefficients for each pairwise variable combination:

$$R = \begin{bmatrix} \rho(A,A) & \rho(A,B) \\ \rho(B,A) & \rho(B,B) \end{bmatrix} = \begin{bmatrix} 1 & \rho(A,B) \\ \rho(B,A) & 1 \end{bmatrix} \tag{3}$$

Since A and B are always directly correlated, the diagonal entries are represented as 1. The diagonal entries are set to 1 by convention, while the off-diagonal entries are correlation coefficients of variable pairs. The values of the coefficients can range from -1 to 1, with -1 representing a direct, negative correlation, 0 representing no correlation, and 1 representing a direct, positive correlation.

The correlation function can also be used to study correlations between variables. This function makes it possible to obtain the values of correlation coefficients as a function of the shift of two variables between each other.

The true cross-correlation sequence of two jointly stationary random variables, x_n and y_n, is given by:

$$R_{xy}(m) = E\{x_{n+m}y_n^*\} = E\{x_n y_{n-m}^*\} \tag{4}$$

where $-\infty < n < \infty$, * denotes the complex conjugation, and E is the expected value operator, $m = 1, 2, 3, \ldots, 2N-1$ and N is maximum length of vector x_n (Stoica and Moses, 2005).

Cross-correlations can thus be calculated as follows:

$$\hat{R}_{xy}(m) = \begin{cases} \sum_{n=0}^{2N-m-1} x_{n+m-N}y_n^* & m \geq N \\ \hat{R}_{yx}^*(-m+N) & m < N \end{cases} \tag{5}$$

In order for the value of cross-correlation to take a value in the range of 0 to 1, normalisation is performed using the formula:

$$\hat{R}_{xy_{\text{normalised}}}(m) = \frac{1}{\sqrt{\hat{R}_{xx}(0)\hat{R}_{yy}(0)}}\hat{R}_{xy}(m) \tag{6}$$

Which means that at zero lag, the cross-correlation is equal to 1.

4 Results

Obtaining test measurement results involved determining the accuracy of methods 2 and 3 based on linear measurements of base sections. The data acquired using method 1 were used as the reference data, since it is the classic method used for a long time, and its accuracy is ±1.5 mm (when measured in three series).

Figure 10 shows all analysed sections (vertical and horizontal) of all three bases: left, middle, and right, marked on the slice of point cloud from Leica TRC360 laser scanner. The figure shows that each of the bases has similar geometry and placement of points to measure the height and width of the chamber.

On the point cloud acquired with the Leica RTC360, the base sections (vertical and horizontal) were measured using two methods:

- measurement 1: directly measuring the distance between base points on the point cloud,

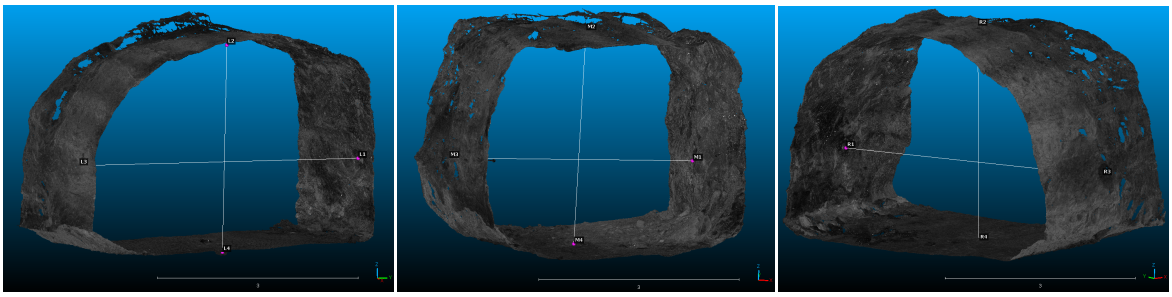

(a) (b) (c)

Figure 10. Slice of point cloud with bases sections: (a) – left, (b) – middle, (c) – right

Table 1. Differences in the lengths of sections measured by methods 1 (Leica Disto) and 2 (Leica TRC360)

Base	Section	Leica Disto [m]	Leica TRC360		Leica Disto – Leica TRC360	
			Measur. 1 [m]	Measur. 2 [m]	Measur. 1 [m]	Measur. 2 [m]
Left	horizontal L1-L3	4.873	4.870	4.873	0.003	0.000
	vertical L2-L4	3.110	3.109	3.109	0.001	0.001
Right	horizontal R1-R3	4.806	4.803	4.807	0.003	-0.001
	vertical R2-R4	3.450	3.446	3.446	0.004	0.004
Middle	horizontal M1-M3	3.862	3.867	3.865	-0.005	-0.003
	vertical M2-M4	3.223	3.223	3.223	0.000	0.000
				Standard deviation:	**0.003**	**0.002**

- measurement 2: determining the coordinates of the base points in the local system, and then calculating the distance between the base points based on the coordinates.

Determining the lengths of the base sections using two methods increased the reliability of the results and the average errors.

On the point clouds acquired with the Motorola G100 smartphone, the base segments (vertical and horizontal) were measured in one way, by determining the coordinates of the base points in the local system of each cloud, and then calculating the distance between the base points based on the coordinates (similar to Measurement 2 for Leica RTC360 data).

4.1 Compatibility of laser rangefinder and laser scanner data

Table 1 shows the results of measuring sections of the bases with a hand-held laser rangefinder and measuring the same sections on a point cloud that was acquired with a laser scanner. In addition, at the end of the table, the differences between the lengths are summarised. Based on these, the standard deviation was calculated, characterising the practical accuracy of the scans (in the case where the quantities measured with the Leica Disto are used as the standard). The standard deviation of the directly measured corresponding sections on the point cloud was 3 mm (measurement 1), while the standard deviation of the lengths of the sections, calculated from the coordinates of the base points, was 2 mm (measurement 2).

Based on the obtained results, it can be concluded that there is a high degree of alignment between the measurements made using the classic method 1 and the data acquired using method 2. The magnitudes of the obtained standard deviations are within the error limit of distance measurement with a hand-held laser rangefinder. Based on the described experiment, it can be concluded that the laser scanning data are sufficiently accurate to be used in the study of the convergence of sidewalk chambers in mine conditions. The resulting point cloud is so dense that even in the absence of texture, and having only reflection intensity, identification of the base points does not pose a problem.

Due to the high metric accuracy of the point cloud acquired with Leica TRC360 scanner, the lengths of the segments between the points of each base measured on this point cloud were taken as a reference. Therefore, in the following part of the study, the data from Leica TRC360 scanner was compared with the results of measurements taken with a smartphone to determine the accuracy of the point clouds resulting from photogrammetric processing of the images.

4.2 Compatibility of laser scanner and smartphone data

In measuring the chamber's three bases, the accuracy of method 3 was determined by comparing its results with those of method 2 . Included in this analysis are the lengths of main base sections (i.e., sections between opposite base points), hereafter referred to as 'main sections'. Also included in this analysis are the lengths of intermediate base sections (i.e. sections between adjacent base points), hereafter referred to as 'intermediate sections'. The distances determined on the point cloud, which were acquired with a Leica TRC360 scanner, were taken as model distances between adjacent points of the bases. This assumption was possible because of the high metric correspondence between the point cloud and the Leica Disto laser rangefinder measurements on the main bases.

Table 2 shows the lengths of the main and intermediate base sections measured on the scans from each series and their discrepancies with the data acquired with Leica TCR360 scanner. Based on

Table 2. The lengths of the main and intermediate base sections measured on the scans acquired with a Motorola G100 from each series and their discrepancies with the data acquired with a Leica TCR360 scanner

Base	Section	Section length [m]			Difference between length and average of three series [m]			Difference between length and reference section (from TLS) [m]		
		Series 1	Series 2	Series 3	Series 1	Series 2	Series 3	Series 1	Series 2	Series 3
Left	L1-L3	4.693	4.725	4.754	0.031	0.001	0.030	0.180	0.148	0.119
	L2-L4	2.972	2.994	3.025	0.025	0.003	0.028	0.138	0.116	0.085
			standard deviation:		0.028	0.002	0.029	0.160	0.133	0.103
	L1-L2	2.780	2.777	2.816	0.011	0.014	0.025	0.111	0.114	0.076
	L2-L3	2.983	3.012	3.030	0.025	0.004	0.022	0.124	0.095	0.077
	L3-L4	2.813	2.853	2.851	0.026	0.014	0.012	0.113	0.073	0.074
	L1-L4	2.559	2.569	2.598	0.017	0.006	0.023	0.103	0.092	0.063
			standard deviation:		0.021	0.010	0.021	0.113	0.095	0.073
						number of photos:		135	139	123
Right	R1-R3	4.687	4.712	4.732	0.023	0.001	0.022	0.119	0.094	0.074
	R2-R4	3.357	3.336	3.388	0.003	0.024	0.027	0.093	0.114	0.062
			standard deviation:		0.017	0.017	0.025	0.107	0.105	0.068
	R1-R2	3.178	3.178	3.194	0.006	0.005	0.011	0.083	0.083	0.067
	R2-R3	3.151	3.100	3.171	0.010	0.041	0.031	0.064	0.115	0.044
	R3-R4	2.637	2.628	2.644	0.000	0.008	0.008	0.068	0.076	0.060
	R1-R4	2.662	2.719	2.721	0.039	0.018	0.021	0.080	0.023	0.021
			standard deviation:		0.020	0.023	0.020	0.074	0.082	0.051
						number of photos:		94	88	72
Middle	M1-M3	3.736	3.700	3.656	0.038	0.003	0.041	0.126	0.162	0.206
	M2-M4	3.124	3.088	3.043	0.039	0.003	0.042	0.099	0.135	0.180
			standard deviation:		0.039	0.003	0.042	0.113	0.149	0.193
	M1-M2	2.553	2.536	2.509	0.020	0.003	0.023	0.109	0.126	0.153
	M2-M3	2.745	2.727	2.706	0.019	0.001	0.020	0.092	0.110	0.131
	M3-M4	2.325	2.301	2.271	0.026	0.002	0.028	0.071	0.095	0.125
	M1-M4	2.170	2.133	2.091	0.039	0.002	0.041	0.061	0.098	0.141
			standard deviation:		0.027	0.002	0.029	0.085	0.108	0.138
						number of photos:		62	108	116

these data, it can be concluded that the agreement between the measurement series is about 2–4 cm. On the other hand, the standard deviation of the length of the sections acquired with a smartphone, when compared to the reference values, is estimated at the level of up to 12 cm. These errors eliminate this simple and mobile method to the tasks of determining the convergence of sidewalk chambers.

The scale of three-dimensional models obtained from photogrammetric processing of Motorola images averages 0.97 (this value was estimated on the basis of relative errors). The models of all three bases generated from the data of all three-measurement series are smaller than the real object by 3%. This is due to the peculiar arrangement of the images in one row and the lack of tie points in the photogrammetric processing of the images. The individual images were taken with the camera travelling along a circular trajectory. Such an arrangement is unfavourable due to the lack of lateral coverage and the alignment problem. The lack of tie points, on the other hand, results in the absence of points with known coordinates in the local system in the alignment process.

In the development of the survey data, an attempt was made to manually indicate the alignment points (without providing their coordinates in the local system) on half of the images included in the alignment. Calculations made using Pix4Dmatic software, did not improve the accuracy of the generated 3D models of the chambers, which confirms the need to stabilise the alignment points on the registered object and the necessity to measure their location in the local system.

4.3 Correlations of smartphone measurements

Based on the collected data, it can be concluded that the differences in the lengths of the sections, measured on the clouds from Motorola G100 smartphone and from Leica TCR360 scanner, depend on:

- the number of images acquired in a single series at the measurement stage and used in post-processing with Pix4Dcloud software – as presented by the graphs in Figure 11 (for main sections) and Figure 12 (for intermediate sections),
- the length of a given section (main or intermediate) – as presented by the graphs in Figure 13 (by measurement series).

The differences between the lengths of the sections on the scans acquired with Leica TCR360 scanner and those acquired with smartphone Motorola G100 tend to increase with the number of images taken using the Pix4Dcatch application. It is significant that all the distances measured on the point clouds, which were generated in Pix4Dcloud for each series, are several centimetres smaller than the reference distances (no distances larger than the reference distances).

The differences between the lengths of the base sections measured on scans made with a laser scanner and the lengths of the base sections measured on scans made with a smartphone are larger for longer sections, and smaller for shorter sections. Thus, noticeably, the accuracy of the base parameters depends on the size of the chamber under study. A confirmation of this statement is provided by the linear increasing trend lines for each series of the graph presented in the figure. It should be noted that each series differs in the number of images used for generating the base point cloud.

Using statistical formulas, the correlation matrix between the deviation from the benchmark value and the size of the base sections and the number of sets of images from which the point clouds of the base models were generated was calculated. The matrix calculated on the basis of all measurement series of all bases has the

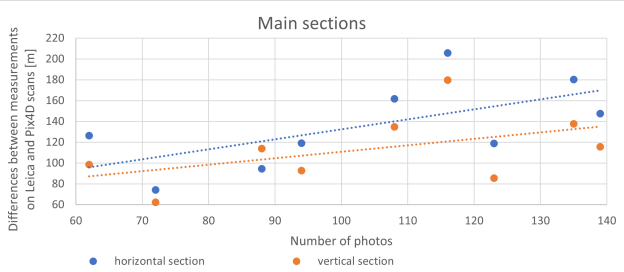

Figure 11. Dependence of the accuracy of measured base main sections on the number of images acquired during base registration in a single series

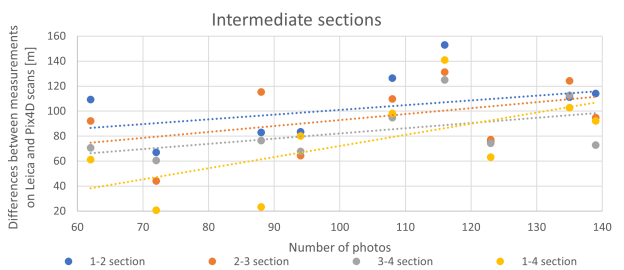

Figure 12. Dependence of the accuracy of measured base intermediate sections on the number of images acquired during base registration in a single series

form:

$$R(L,D) = \begin{bmatrix} 1 & 0.3256 \\ 0.3256 & 1 \end{bmatrix} \tag{7}$$

$$R(F,D) = \begin{bmatrix} 1 & 0.4281 \\ 0.4281 & 1 \end{bmatrix} \tag{8}$$

where L is length of sections of the base (main and intermediate), D is the difference between reference length measured on the Leica TCR360 data, and length measured on the Motorola G100 data [mm], where F is the number of photos in a given series of registration with a smartphone Motorola G100.

The elements of the matrix on the first diagonal are 1, because the variables L, D, and F are directly correlated with each other. The elements of the matrix on the second diagonal are the correlation coefficients of the pairs of variables L, D and L, F. The values of the coefficients of pairs of variables are in the range from 0 to 1, so they indicate a positive correlation of these variables. Therefore, it can be concluded that the accuracy and metricity of scans acquired with smartphone Motorola G100 depends on both the number of images captured in one series and the size of the object.

Moreover, the closer the value of the correlation coefficient to 1, the stronger the positive correlation. Therefore, it can be concluded that the accuracy and metricity of scans acquired with smartphone Motorola G100 depend more on the number of images taken than on the size of the chamber. The statistics support the conclusions drawn from the analysis of the charts presented in Figure 11, Figure 12, and Figure 13.

Using the ranks of the L, D and F vectors, i.e., deviations from the benchmark value, the magnitude of the lengths of the base sections, and the abundance of the image sets obtained in each measurement session, the values of the cross-correlation function were calculated. Unfortunately, it was only possible to estimate the sequence, since in practice only a finite segment of one realisation of an infinitely long random process is available. However, based on the correlation plots of the discrete sequences, it is possible to infer the similarity of the analysed signals.

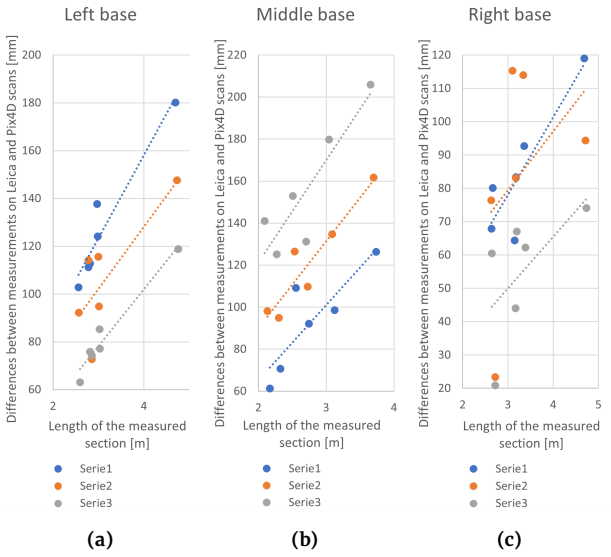

Figure 13. Dependence of the accuracy of measured base intermediate sections on the length of these sections (main and intermediate)

Figure 14 shows the normalised cross-correlation between the deviation of scans acquired with smartphone Motorola G100 from a scan acquired with a Leica TCR360 scanner and two parameters:

- length of each section of the base (main and intermediate) – Figure 14a,
- the number of photos in a given series of registration with smartphone Motorola G100 with Pix4Dcatch – Figure 14b.

The cross-correlation is calculated as the sum of the values of the two signals multiplied by each other, according to equation (5). Correlation calculations are performed for different values of time shift (lag). One of the signals is shifted relative to the other, and for each shift we multiply the overlapping samples by each other and add up the results. The cross-correlation is very similar to splicing. The shape of the graph of the correlation function indicates the uniformity of the change in the value of one vector and the change in the value of the other vector. Based on the observation of the points of the function, it can be determined whether the similarity of the vectors is linear or nonlinear.

In two graphs presented in Figure 14, the maximum value of cross-correlation for a lag equal to 0 indicates the absence of a shift between sets of variables. It should be noted that tto its axis (i.e., the vertical line intersecting the x-axis at point 0) than the graph in Figure 14b. This shows that as vector D increases, vector L changes more uniformly than vector F. This conclusion proves that section length errors change with the change in section length more evenly than with the change in the number of images. Therefore, the analysis of the cross-correlation results also confirms the existence of a scaling factor for the point clouds that were acquired in post-processing.

4.4 Comparative analysis of point clouds from laser scanner and smartphone

Based on the above statistical analysis, the degree of influence of two parameters of the 3D model on its accuracy was determined: the size of the object and the size of the data recorded with a Motorola G100 smartphone. This analysis is based only on the linear sizes of the individual base sections and includes an overall comparison of the two types of 3D models.

Using CloudCompare software, the point clouds that were created from the sets of images acquired in all measurement series

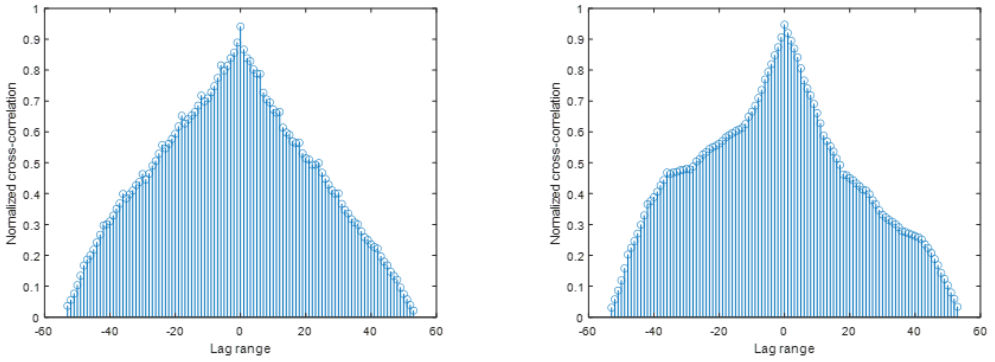

(a) (b)

Figure 14. Cross-correlation between the deviation of scans acquired with a smartphone Motorola G100 from scan acquired with a Leica TCR360 scanner and: (a) – length of each section of the base (main and intermediate), (b) – the number of photos in a given series of registration with a smartphone Motorola G100 with Pix4Dcatch

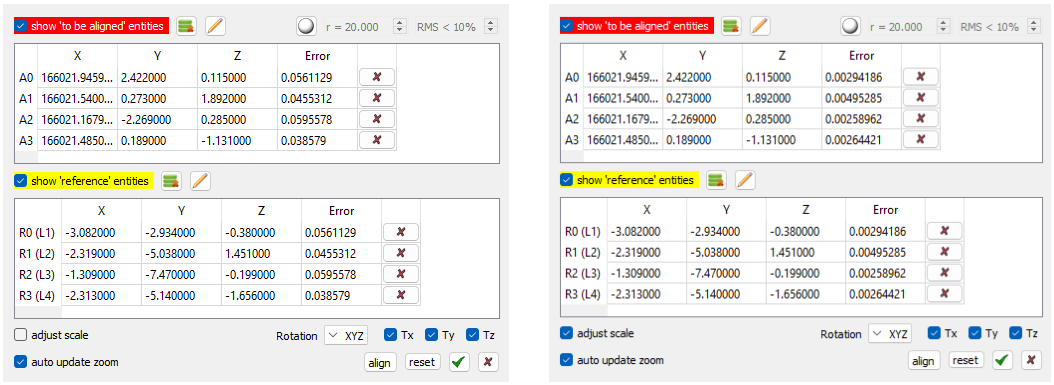

(a) (b)

Figure 15. Tie points error of registration point cloud from Pix4Dcloud to point cloud from Leica TCR360 based on four base points (metal pins) in two variants: (a) – disregarding a scale factor, (b) – using a scale factor

of the left base were compared with the point cloud that was registered with Leica TRC360 scanner. The comparison was made by registering the point cloud from Pix4Dcloud into the point cloud from the Leica TCR360 based on four base points (metal pins) in two variants:

- without a scale factor – a rigid fit that does not adapt to the shape of the base,
- with a scale factor (the same in all directions of the axis of the coordinate system) – a flexible fit, which adapts to the shape of the base.

Figure 15 shows the results of an example registration of point cloud from Pix4Dcloud (in series 1) to a point cloud from Leica TCR360 in two alignment variants: (a) – disregarding the scale factor and (b) – using the scale factor. The alignment errors of all four tie points are on average twenty times smaller after calculating the transformation parameters as a result of alignment in the second variant than after calculating the transformation parameters as a result of alignment in the first variant.

In turn, Figure 16 shows the point cloud slices after registration with the scale factor. This is the cloud generated in post-processing from a set of images of the left base. It was registered with a scale factor considering four base points. The post-processed cloud was then compared with the point cloud acquired with Leica TCR360 scanner. The comparison was made automatically with CloudCompare software using the "cloud to cloud" function. The computational model involves calculating the distance of the point of the first cloud from the plane passing through the nearest point of the second cloud and its neighbourhood. The plane is calculated by the method of least squares.

The colour tones show the discrepancies between the point cloud from Leica TCR360 scanner and the point cloud from Motorola G100 smartphone, acquired in the first (presented in Figure 16a), second (presented in Figure 16b), and third (presented in Figure 16c) measurement series. The base points (metal pins) and the main sections of the base are marked on each slice. Next to the slice, the parameters of the equalisation are presented: final RMS, transformation matrix with shift vector and scale factor. These parameters were determined in the process of fitting three-point clouds (from three series) of the same left base.

It should be noted that the maximum values of distances occur only for individual points, which can be understood as fatal errors. Using histograms, which show the distribution of individual distances (from 0 to max) according to the number of points of the analysed cloud that have the characteristics of the corresponding distances, it is possible to read the practical ranges of distances, which, represented by the overwhelming majority, are as follows: 0–0.010 – for point cloud measured in first series, 0–0.012 – for point cloud measured in second series, 0–0.011 – for point cloud measured in third series. Meanwhile, the scale factors obtained for the data in each series are: 1.04077, 1.03205, and 1.02530. These values confirm the absolute error calculated earlier. The point clouds, obtained in post-processing, are scaled with respect to the dimensions of the actual chamber.

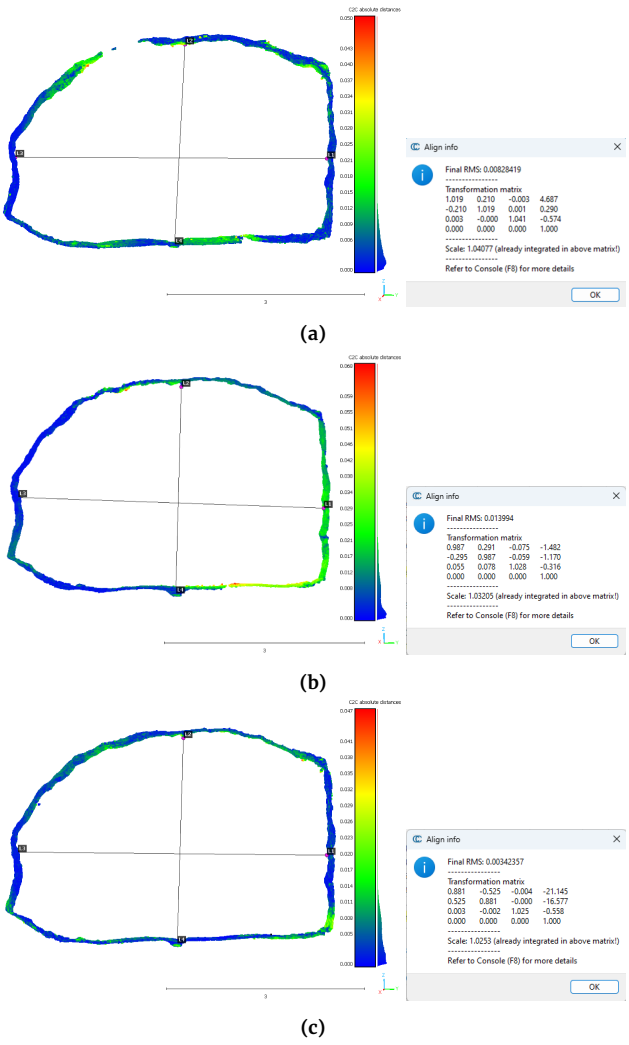

Figure 16. Slices Comparison of point clouds acquired from images taken with smartphone Motorola G100 (analysed data) and a point cloud that was acquired with Leica TCR360 (reference data). The distances between the cloud points, which were calculated automatically in CloudCompare software using the ”cloud-to-cloud” function, are shown in colour tones. Data of left base from: (a) – series 1, (b) – series 2, (c) – series 3

5 Discussion

Considering the design of the devices used (laser scanner, smartphone and iPad), the compact and lightweight solutions are economical and highly functional in difficult underground conditions. Moreover, they can be used for three-dimensional interpretation of the geometry of the surveyed object.

The evaluation of the accuracy of data from Leica RTC360 3D laser confirms that laser scanning technology is as precise as Leica Disto hand-held laser rangefinder measurement currently used in "Kłodawa" salt mine. Theoretically, the accuracy of the first method is estimated at 1.9 mm (3D point accuracy at 10 m), while the second method is estimated at ± 2.5 mm (considering targeting and touchdown errors in one measurement series). The research has shown that the accuracy of measuring the length of sections of bases at the required level of 1–2 mm is achievable using Leica RTC360 3D laser scanner.

In addition, the appropriateness of laser scanning technology is justified by its high accuracy and the possibility of three-dimensional analysis of changes occurring in mine formations. Unlike classical convergence measurements, which allow for the determination of changes in the width and height of the bases, point cloud comparison allows for the determination of changes in any direction of the three-dimensional coordinate system. Such a solution should be pursued by modernising the methodology for measuring the degree of deformation of salt chambers

The research described in this article also involved testing low-cost, mobile, and innovative technologies for capturing 3D data in mine conditions. The demonstrated measurements were taken using the PIX4Dcatch and 3d Scanner application. This software allows for the registering of objects as point clouds. This specialised software implemented in any smartphone, facilitates the acquisition of scans during photogrammetric image processing executed either on the smartphone mobile camera or in direct measurement performed using the iPhone's LiDAR sensor.

Unfortunately, using an iPad with a built-in LiDAR sensor and equipped with appropriate software, it was not possible to obtain satisfactory results, because of the lack of adequate lighting, homogeneity of colour and shape of the measured chamber, as well as dusty air. Presumably, changing these parameters could improve the result of data acquisition using an iPad with LiDAR.

As a result of automatic post-processing of a set of photos taken with a commonly used smartphone, a quasi-continuous representation of the measured object was obtained from the form of a point cloud. The measurements were made in three series, on three bases of different sizes. This made it possible to establish cyclicity and eliminated the randomness of the data obtained. On the basis of the tests, the accuracy of the point clouds obtained in the results of image matching was found to be several centimetres. Such large errors are due to the lack of tie points in the alignment processwhile the obvious advantage of the method is that it is quick to apply and intuitive.

The point clouds generated by photogrammetric processing of smartphone images are scaled to the size of the real object. This conclusion was confirmed by the graphs presented in the figure, as well as the statistical analysis of the relationship of the L, D, and F variables. The correlations suggest the possibility of the existence of a constant scale factor of the point clouds, which were obtained through post-processing of the set of photos. The size of this coefficient is determined primarily by the size of this collection. The function of this relationship should be understood better with further research.

6 Conclusions

Based on the measurements and their analysis, it can be concluded that method 2 is as accurate as method 1, which is commonly used in salt mines. The lengths of the main base sections, determined indirectly (by calculating them from the coordinates of the base points) or directly (by measuring them) on the point cloud with Leica TCR360, differ by 2–3 mm from the lengths of the sections measured with Leica Disto hand-held laser rangefinder. It is worth mentioning that the accuracy of a single measurement with Leica Disto is estimated to be within 2 mm. The method of stationary laser scanning can be recommended as a method with sufficient accuracy to measure the bases in the pits of salt mines.

The analyses presented in this article indicate that it is not possible to use the proposed method 3 and method 4, which involve fast and inexpensive mapping of objects in the form of point clouds, for precise convergence measurements. The data are non-metric, and the scale of three-dimensional models is not preserved, due to the lack of reference points. Statistical analyses of the data, which were acquired using a Motorola G100 smartphone, indicate low measurement accuracy of up to 19 cm. The error in the length of the base sections is proportionally dependent on the length of the sections, but also on the number of images taken. Correlation analyses and the calculated Pearson linear correlation coefficients, despite the burden of outliers, indicate the presence of a scale factor in the measurement material. To draw conclusions at a satisfactory level of

Pearson linear correlation. A statistical analysis of the data, which were acquired with iPad Pro with LiDAR technology using several applications, was not undertaken. During the registration of the bases in the sidewalk chambers, each time point clouds were obtained with a density that made it impossible to identify the points of the bases. The point clouds had gaps, deficiencies, and displacement between their parts.

References

Adamek, A. (2015). Mobilna Platforma Górnicza (MPG) – nowatorskim rozwiązaniem w polskich kopalniach (Mobile Mining Platform – an innovative solution in Polish mines). *Archiwum Fotogrametrii, Kartografii i Teledetekcji*, pages 11–24, doi:10.14681/afkit.2015.001.

Baltsavias, E. P. (1999). A comparison between photogrammetry and laser scanning. *ISPRS Journal of Photogrammetry and Remote Sensing*, 54(2–3):83–94, doi:10.1016/s0924-2716(99)00014-3.

Błaszczak-Bąk, W., Suchocki, C., Kozakiewicz, T., and Janicka, J. (2023). Measurement methodology for surface defects inventory of building wall using smartphone with light detection and ranging sensor. *Measurement*, 219:113286, doi:10.1016/j.measurement.2023.113286.

Benito-Calvo, A., Gutiérrez, F., Martínez-Fernández, A., Carbonel, D., Karampaglidis, T., Desir, G., Sevil, J., Guerrero, J., Fabregat, I., and García-Arnay, A. (2018). 4D monitoring of Active Sinkholes with a Terrestrial Laser Scanner (TLS): A case study in the Evaporite Karst of the Ebro Valley, NE Spain. *Remote Sensing*, 10(4):571, doi:10.3390/rs10040571.

Bieniasz, J., Ciągło, W., and Wojnar, W. (2003). Nowa metoda pomiarów deformacji solnej struktury filarowo-komorowej wykorzystująca dalmierz laserowy (A new method for measuring the deformation of a salt pillar-chamber structure using a laser rangefinder). *Geodezja/Akademia Górniczo-Hutnicza im. Stanisława Staszica w Krakowie*, 9(2/1):187–193.

Bieniasz, J. and Wojnar, W. (2007). Zarys historii pomiarów i wybrane wyniki obserwacji zjawiska konwergencji wyrobisk w pokładowych złożach soli (An outline of the history of measurements and selected results of observations of the phenomenon of convergence of workings in seam salt deposits). *Gospodarka Surowcami Mineralnymi*, 23:133–142.

Corradetti, A., Seers, T., Billi, A., and Tavani, S. (2021). Virtual outcrops in a pocket: The smartphone as a fully equipped photogrammetric data acquisition tool. *GSA Today*, 31(9):4–9, doi:10.1130/gsatg506a.1.

Dorninger, P., Nothegger, C., Pfeifer, N., and Molnár, G. (2008). On-the-job detection and correction of systematic cyclic distance measurement errors of terrestrial laser scanners. *Journal of Applied Geodesy*, 2(4), doi:10.1515/jag.2008.022.

El-Din Fawzy, H. (2019). Study the accuracy of digital close range photogrammetry technique software as a measuring tool. *Alexandria Engineering Journal*, 58(1):171–179, doi:10.1016/j.aej.2018.04.004.

Gollob, C., Ritter, T., Kraßnitzer, R., Tockner, A., and Nothdurft, A. (2021). Measurement of forest inventory parameters with Apple iPad Pro and integrated LiDAR technology. *Remote Sensing*, 13(16):3129, doi:10.3390/rs13163129.

Huang, X., Zhang, Y., and Xiong, Z. (2021). High-speed structured light based 3D scanning using an event camera. *Optics Express*, 29(22):35864, doi:10.1364/oe.437944.

Jankowska, I. and Kwaśniak, M. (2015). Rola dokładności wyznaczania konwergencji wyrobisk w aspekcie zagospodarowania pustek poeksploatacyjnych w kopalniach soli (Role of accuracy in determining the convergence of workings with regard to managing post-excavation spaces in salt mines). In Kwaśniak, M., editor, *Techniki inwentaryzacji i monitoringu obiektów inżynierskich*, pages 32–43. Warsaw University of Technology, Faculty of Geodesy and Cartography, Engineering Geodesy and Control Surveying Systems.

Jaud, M., Kervot, M., Delacourt, C., and Bertin, S. (2019). Potential of smartphone SfM photogrammetry to measure coastal morphodynamics. *Remote Sensing*, 11(19):2242, doi:10.3390/rs11192242.

Kortas, G., Szewczyk, J., and Toboła, T. (2004). *Ruch górotworu i powierzchni w otoczeniu zabytkowych kopalń soli (Movement of the rock mass and surface in the vicinity of historic salt mines)*. Wydaw. Instytutu Gospodarki Surowcami Mineralnymi i Energią PAN.

Kottner, S., Thali, M. J., and Gascho, D. (2023). Using the iPhone's LiDAR technology to capture 3D forensic data at crime and crash scenes. *Forensic Imaging*, 32:200535, doi:10.1016/j.fri.2023.200535.

Kukutsch, R., Kajzar, V., Konicek, P., Waclawik, P., and Ptacek, J. (2015). Possibility of convergence measurement of gates in coal mining using terrestrial 3D laser scanner. *Journal of Sustainable Mining*, 14(1):30–37, doi:10.1016/j.jsm.2015.08.005.

Kunstman, A., Poborska-Młynarska, K., and Urbańczyk, K. (2002). *Zarys otworowego ługownictwa solnego: aktualne kierunki rozwoju (Outline of borehole salt leaching: current development directions)*. AGH Akademia Górniczo-Hutnicza, Uczelniane Wydawnictwa Naukowo-Dydaktyczne, Karków.

Kurdek, D. (2020). Pomiary konwergencji wyrobisk chodnikowych w Kopalni Soli „Kłodawa" S.A. (Convergence measurements of drift excavation in Salt Mine „Kłodawa" S.A). *Salt Review*, 15:56–61.

Lipecki, T., Jaśkowski, W., Gruszczyński, W., Matwij, K., Matwij, W., and Ulmaniec, P. (2016). Inventory of the geometric condition of inanimate nature reserve Crystal Caves in "Wieliczka" Salt Mine. *Acta Geodaetica et Geophysica*, 51:257–272, doi:10.1007/s40328-015-0125-5.

Lipecki, T. and Thi Thu Huong, K. (2020). The development of terrestrial laser scanning technology and its applications in mine shafts in Poland. *Inżynieria Mineralna*, 1(2), doi:10.29227/im-2020-02-36.

Litoński, A. (1960). Przepisy technicznej eksploatacji kopalń soli (Regulations on the technical operation of salt mines). Technical report, Ministerstwo Przemysłu Chemicznego, Wydawnictwo Górniczo–Hutnicze, Katowice, Poland.

Lohani, B. and Ghosh, S. (2017). Airborne LiDAR technology: A review of data collection and processing systems. *Proceedings of the National Academy of Sciences, India Section A: Physical Sciences*, 87(4):567–579, doi:10.1007/s40010-017-0435-9.

Maj, A. (2011). Konwergencja w warunkach nieregularnie rozproszonych wyrobisk, na przykładzie kopalni wieliczka (Convergence in conditions of irregularly dispersed workings, on the example of the Wieliczka mine). *Prace Instytutu Mechaniki Górotworu PAN*, 13(1-4):121–130.

Maj, A. and Florkowska, L. (2013). Obserwacja oddziaływania wyrobisk na powierzchnię terenu w warunkach kopalń soli (Observation of the impact of excavations on the ground surface in the conditions of salt mines). *Prace Instytutu Mechaniki Górotworu PAN*, 15(3-4):107–113.

Miller, S. H., Hashemian, A., Gillihan, R., and Helms, E. (2022). A comparison of mobile phone LiDAR capture and established ground based 3D scanning methodologies. In *SAE Technical Paper Series*, ANNUAL. SAE International, doi:10.4271/2022-01-0832.

Ochalek, A. (2018). Analysis of convergence and deformation measurements based on classical geodetic surveys and terrestrial laser scanning in Wieliczka salt mine. In *18th International Multidisciplinary Scientific GeoConference SGEM2018, Informatics, Geoinformatics and Remote Sensing*, SGEM2018. Stef92 Technology, doi:10.5593/sgem2018/2.2/s09.073.

Pearson, K. (1896). Mathematical contributions to the theory of evolution. iii. regression, heredity, and panmixia. *Philosophical Transactions of the Royal Society of London. Series A*, (187):253–318.

Poborska-Młynarska, K. (2022). *Geologiczno-górnicze warunki*

eksploatacji w kopalniach podziemnych w wysadach solnych Polski środkowej (Geological and mining operating conditions in underground mines in salt domes in central Poland). AGH Akademia Górniczo-Hutnicza, Uczelniane Wydawnictwa Naukowo-Dydaktyczne, Karków.

Regulation (1970). Zarządzenie zewnętrzne nr 18 Naczelnego Dyrektora Kopalni Soli „Kłodawa" z dnia 1 kwietnia 1970 r. dotyczące wprowadzenia „instrukcji/tymczasowej/ w sprawie określenia stanu zagrożenia wodnego kopalni oraz organizacji środków i służby dla ochrony załogi i ruchu kopalni" (External Order No. 18 of the General Director of the "Kłodawa" Salt Mine of April 1, 1970 regarding the introduction of "temporary instructions on determining the state of water hazard in the mine and organizing measures and services to protect the crew and mine operations").

Rutkowski, W. and Lipecki, T. (2023). Use of the iPhone 13 Pro LiDAR scanner for inspection and measurement in the mineshaft sinking process. *Remote Sensing*, 15(21):5089, doi:10.3390/rs15215089.

Sapirstein, P. (2016). Accurate measurement with photogrammetry at large sites. *Journal of Archaeological Science*, 66:137–145, doi:10.1016/j.jas.2016.01.002.

Stoica, P. and Moses, R. L. (2005). *Spectral analysis of signals*, volume 452. Pearson Prentice Hall Upper Saddle River, NJ.

Suchocki, C., Katzer, J., and Panuś, A. (2017). Remote sensing to estimate saturation differences of chosen building materials using terrestrial laser scanner. *Reports on Geodesy and Geoinformatics*, 103(1):94–105, doi:10.1515/rgg-2017-0008.

Suchocki, C., Okrój, S., and Błaszczak-Bąk, W. (2023). Methodology for the measurement and 3D modelling of cultural heritage: a case study of the monument to the Polish Diaspora Bond with the Homeland. *Reports on Geodesy and Geoinformatics*, 116(1):1–8, doi:10.2478/rgg-2023-0005.

Świerczyńska, E. (2020). Reprezentatywność kształtu obiektu odwzorowanego za pomocą "chmury punktów" – analiza na podstawie danych z technologii wideotachimetrycznej (Representativeness of the shape of an object mapped using a "point cloud" – analysis based on data from video tachymetry technology). *Przegląd Geodezyjny*, 1(4):23–27, doi:10.15199/50.2020.4.3.

Świerczyńska, E. and Kołakowska, M. (2014). The attempt to use levelling rods for testing metric properties of surveying instruments, which are used for reflectorless distance measurements. *Reports on Geodesy and Geoinformatics*, 96(1):38–54, doi:10.2478/rgg-2014-0005.

Szafarczyk, A. and Gawałkiewicz, R. (2018). Defining the cubature changes of historic St. Kinga Chamber in Bochnia salt mine, using laser scanning technology. *E3S Web of Conferences*, 35:04006, doi:10.1051/e3sconf/20183504006.

Teppati Losè, L., Spreafico, A., Chiabrando, F., and Giulio Tonolo, F. (2022). Apple LiDAR sensor for 3D surveying: Tests and results in the cultural heritage domain. *Remote Sensing*, 14(17):4157, doi:10.3390/rs14174157.

Teukolsky, S. A., Flannery, B. P., Press, W., and Vetterling, W. (1992). Numerical recipes in c. *SMR*, 693(1):59–70.

Woźniak, M., Świerczyńska, E., and Jastrzębski, S. (2015). The use of video-tacheometric technology for documenting and analysing geometric features of objects. *Reports on Geodesy and Geoinformatics*, 99(1):28–43, doi:10.2478/rgg-2015-0010.

Zaczek-Peplinska, J. (2023). Pomiary inwetaryzacyjne z wykorzystaniem Apple iPhone 13 Pro i zintegrowanej technologii LiDAR (Inventory measurements using Apple iPhone 13 Pro and integrated LiDAR technology). *Przegląd Geodezyjny*, 1(2):16–19, doi:10.15199/50.2023.02.1.